JOURNAL OF Materials CHEMISTRY

Influence of electrochemical processing on the composition and microstructure of chemical-vapor deposited Ru and RuO_2 nanocrystalline films

Simona Barison,[a] Davide Barreca,[b] Sergio Daolio,[a] Monica Fabrizio*[a] and Eugenio Tondello[b]

[a]*IENI CNR, Corso Stati Uniti 4, I-35127 Padova, Italy. E-mail: m.fabrizio@ipelp.pd.cnr.it; Fax: +39 049 829 5853*
[b]*ISTM CNR, Dipart. CIMA, Università di Padova, Via Marzolo 1, I-35131 Padova, Italy*

Received 19th November 2001, Accepted 30th January 2002
First published as an Advance Article on the web 20th March 2002

Modifications of nanocrystalline RuO_2 and Ru films, chemical-vapor deposited on Ti substrates, are studied in aqueous media, at the initial stages of electrocatalytic O_2 evolution. The microstructure, composition and morphology of the films are examined *ex situ* by X-ray diffraction (XRD), X-ray photoelectron spectroscopy (XPS), secondary ion mass spectrometry (SIMS) and atomic force microscopy (AFM). Results concerning the influence of electrochemical processing on the chemico-physical properties and electrode behavior are presented and discussed.

Introduction

Materials based on Ru and RuO_2 have come under intense scrutiny over the last two decades for electrochemical, catalytic and electronic applications. In particular, the increasing technological importance of electrocatalytic gas evolution reactions (oxygen, chlorine, hydrogen) has promoted many investigations aimed at obtaining more efficient electrodes and, as tested for some other noble metals and their oxides, Ru and RuO_2 were confirmed to be suitable materials for these purposes.[1]

Ruthenium can also play an important role in electrocatalysis in the metallic state, mainly in the synthesis of oxygen and chlorine. In the potential range for gas evolution, Ru is covered with an oxidic layer that constitutes the electrochemically active material.[2]

RuO_2 has been widely tested in the production of corrosion-resistant electrodes for chlorine synthesis. Moreover, RuO_2 shows a very low overpotential for oxygen evolution in anodic water electrolysis. Nevertheless, it is well known that Ru and RuO_2 exhibit some mechanical fragility and are very expensive. As a consequence, in order to obtain dimensionally stable anodes (DSA®), most studies have been focused on the use of mixed oxide thin films containing valve metals, like Ti, Ta, *etc.* These composites prove advantageous because they combine electrocatalytic activity with the increased chemical and mechanical stability provided by the valve metal.[3] In this context different synthetic routes[4] have been directed towards the preparation of nanocrystalline materials whose high surface-to-volume ratio is generally expected to improve electrode performance.

RuO_2-based electrode films are usually obtained by thermal decomposition of a solution containing a suitable Ru precursor (generally $RuCl_3 \cdot xH_2O$) with Ti alkoxide on a Ti substrate.[5] In this sense, chemical vapor deposition (CVD) can be a valuable alternative synthetic route to Ru- and RuO_2-based thin layers since it offers satisfactory coverage, relatively mild processing conditions and compatibility with the needs of large-scale fabrication, together with accurate control of the purity and microstructure of the films.

This paper is focused on the influence of electrochemical processing on the chemico-physical properties of Ru and RuO_2 nanocrystalline films obtained by CVD from an η^3-allylic ruthenium(II) precursor.[6]

The study was limited to the initial stage of O_2 evolution and the electrochemical activity was tested by means of cyclic voltammetry measurements, evaluation of service life being beyond the scope of this work. Compositional and microstructural and morphological modifications induced by electrochemical tests on the materials were studied *ex situ* by X-ray diffraction (XRD), X-ray photoelectron spectroscopy (XPS), secondary ion mass spectrometry (SIMS) techniques and atomic force microscopy (AFM).

Experimental

Film synthesis

The RuO_2 and Ru films were obtained *via* CVD on one face of metallic titanium discs at a temperature of 300 °C from Ru(COD)(η^3-allyl)$_2$ (COD = cycloocta-1,5-diene) in a custom-built cold wall reactor with a resistively heated susceptor.[6] The Ti substrates (Goodfellow, Cambridge, UK, 99.6+%) were etched, as described below, before CVD in order to improve film adhesion and conductivity by lowering the TiO_2 content on the Ti surface.[7] Titanium substrates were ultrasonically rinsed in a trichloroethylene bath for 15 min, dipped in boiling oxalic acid for 20 min and finally washed with acetone before being introduced into the reactor. The as-deposited films were submitted to voltammetric cycling without further thermal treatments.

Table 1 lists the synthetic and electrochemical conditions used for the RuO_2 and Ru samples studied in the present work, together with their thickness and roughness.

Electrochemical measurements

The cyclic voltammetry measurements were performed on a PAR (Princeton, USA) potentiostat–galvanostat Mod. 263A, controlled by EG&G PARC M270 software. The experiments were carried out in a three-electrode, single-body cell. All the electrode potential values were measured and reported with respect to a saturated calomel electrode (SCE) as reference.

The working electrode was a Ru or RuO_2 film deposited on

Table 1 Synthetic conditions and electrochemical behavior of the RuO_2 and Ru samples

Sample	Composition	Synthetic conditions[a]	Electrochemical conditions	Thickness/μm[b]	R_{ave}/nm[c]
1	RuO_2	O_2	—	1.0	68
2	RuO_2	O_2	Cycled in NaOH (1 M)	0.5	133
3	RuO_2	O_2	Cycled in H_2SO_4 (1 M)	1.7	104
4	RuO_2	O_2	Polarized at +1.2 V for 30 min in H_2SO_4 (1 M)	0.6	119
5	RuO_2	O_2	Polarized at +1.2 V for 30 min in NaOH (1 M)	0.3	105
1m	Ru	N_2	—	1.0	80
2m	Ru	N_2	Cycled in NaOH (0.1 M)	0.7	50
3m	Ru	N_2	Cycled in NaOH (1 M)	—	90

[a]All gases at a pressure of 10 mbar. [b]Thickness was measured by means of the profiler. [c]Average roughness (R_{ave}) was measured by the AFM technique.

one face of a Ti disc ($A_{geom} = 1.54\ cm^2$). Electrical contact was made by soldering a wire on the disc. The counter electrode was a Pt coil around the working electrode. Before each experiment the solution was stirred mechanically and nitrogen was bubbled through it.

X-Ray diffraction (XRD)

Diffraction patterns of thin film samples were collected using a Philips (Eindhoven, NL) PW 1820 diffractometer (Cu-Kα radiation, 40 kV, 50 mA) equipped with a thin film attachment (glancing angle = 0.5°). The average crystallite sizes were estimated by the Debye–Scherrer equation.

X-Ray photoelectron spectroscopy (XPS)

A Perkin-Elmer (Norwalk, USA) Φ 5600ci spectrometer, with monochromatic Al-Kα radiation (1486.6 eV), was used for the XPS analyses performed at pressures lower than 1.8×10^{-9} mbar. The spectrometer was calibrated by assuming the bind- ing energy (BE) of the Au $4f_{7/2}$ line at 84.0 eV with respect to the Fermi level. Detailed scans were run for the following regions: O1s, C1s, Ru3d (pass energy = 5.85 eV; 0.050 eV $step^{-1}$; 100 ms $step^{-1}$). After a Shirley-type background subtraction, the raw spectra were fitted with a non-linear least-square fitting program, adopting Gaussian–Lorentzian peak shapes for all the peaks. The atomic compositions were evaluated using sensitivity factors provided by the Φ V5.4A software.

Secondary ion mass spectrometry (SIMS)

SIMS analyses were carried out in a custom-built instrument as described elsewhere[8] and recently updated. A monochromatic (6 keV) O_2^+ ion beam collimated to 50 μm was generated in a mass-filtered duoplasmatron ion gun (model DP50B, VG Fisons, Loughborough, UK). A quadrupole mass analyzer (Mod. EQS1000, Hiden, Manchester, UK) with a secondary electron multiplier (90° off-axis) was used for positive-ion detection in counting mode. Lens potentials, quadrupole electronic control units and the detection system were controlled *via* a Hiden HAL IV interface. Two personal computers were used to control the instrument, to collect data and to position the sample. The ionic current range was between 400 and 800 nA and constant during the experiments.

Surface characterization was carried out by recording mass spectra of the positive ions at different points on the films, in order to check the compositional homogeneity. Subsequently, by following the signals of interest as a function of sputtering time, the distributions of ion species were studied from the surface to the bulk region and at the coatings–substrate interface. The erosion rate was estimated to be around 20 nm min^{-1} by measuring SIMS crater depths. Border effects were avoided with the electronic gating: only a percentage (from 10 up to 20%) of the rastered area contributed to the ionic signals, which was limited to the central part of the crater.

Since the quadrupole mass resolution is ±1, the ion species were identified by resolving the overlapped *m*/*z* signals with an isotope pattern simulation program. In this way, the confidence interval and residual standard deviations could be calculated for detected ion groups, in order to distinguish their various contributions.

In order to test the compositional homogeneity, SIMS analyses were carried out on different zones of each sample.

Atomic force microscopy (AFM) and profiler analysis

AFM images were taken using a Park Autoprobe CP (Bicester, UK) instrument operating in contact mode in air. The background was subtracted from the images using ProScan 1.3 software from Park Scientific. The electrochemically-processed films were rinsed with distilled water before performing AFM analysis. Depth measurements were performed with a P10 profiler (KLA-Tencor Corp., Milpitas, CA). The film thickness measurements were estimated from the SIMS crater depths.

Results and discussion

The thickness, roughness and composition of the RuO_2 and Ru films were analyzed before and after the electrochemical tests, revealing very similar features for the samples obtained under the same synthetic conditions. The as-deposited RuO_2 films became bluish-black, while the Ru coatings were grey and reflecting. In the following discussion, samples **1** and **1m** are considered to be the prototypes for the as-grown films.

X-Ray diffraction

Fig. 1 shows the XRD spectra, between 10 and 80°, for the as-grown RuO_2 (Fig. 1a) and Ru (Fig. 1b) films. Spectrum (a) indicated the presence of tetragonal RuO_2 as the only crystalline phase, with a strong (101) preferential orientation†. A different film texture, (110), would be expected under equilibrium-like conditions, *e.g.* high substrate temperatures, since the (110) surface is the thermodynamically most stable one for rutile-type structures. This observation indicated that under these synthetic conditions kinetic control of film growth occurred.[9]

Pattern (b) shows the reflections corresponding to metallic Ru with a hexagonal structure‡ and no appreciable orientation

†Pattern no. 40-1290 on JCPDS-ICDD (Joint Committee on Powder Diffraction Standards—International Center for Diffraction Data), 1992.

‡Pattern no. 6-663 on JCPDS-ICDD, 1992.

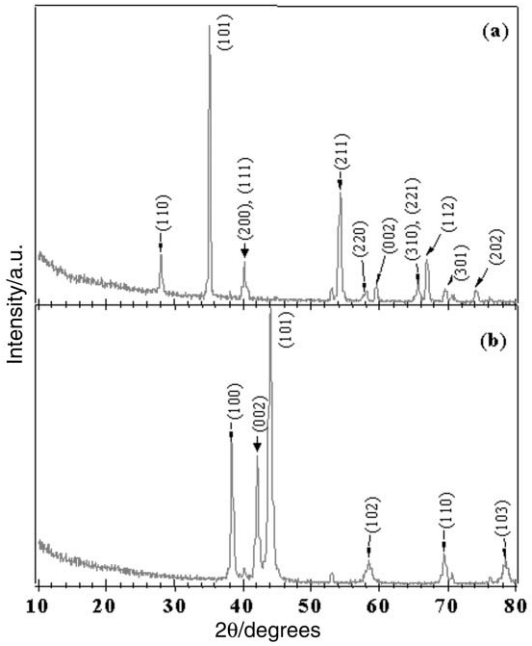

Fig. 1 XRD spectra, over the range $2\theta = 10$–$80°$, for the as-grown (a) RuO_2 and (b) Ru films.

effects. The average crystallite size, calculated from the most intense peak of each spectrum, was estimated to be (20 ± 3) nm for the RuO_2 film and (16 ± 3) nm for the Ru film.

Electrochemical processing

The RuO_2 films were tested both in alkaline (NaOH, 1 M, the usual medium for O_2 electrocatalytic evolution) and acidic media (H_2SO_4, 1 M) at 298 K, in order to assess the influence of the electrolyte on their composition and morphology.

The cyclic voltammetric experiments were carried out between $E = -0.19$ (the open circuit potential for the electrode dipped in NaOH, 1 M) and $E_{an} = +1.00$ V *vs.* SCE, where O_2 bubbles were visible on the electrode surfaces in both electrolytes. In this potential range, the electrodes, cycled for 2 h at 2 mV s^{-1}, showed electrochemical stability in both of the electrolytes, but the film thickness was affected differently. With respect to the as-grown RuO_2 (compare with sample **1** in Table 1), the cycled film became thinner in NaOH (1 M) but thickened in H_2SO_4 (1 M). With the electrodes polarized at +1.20 V, the reported potential for O_2 evolution on polycrystalline RuO_2,[10] vigorous bubbling was visible and the thinning effect was observed in both alkaline and acidic media.

The different reaction pathways occurring in either alkaline or acidic media can explain these effects. The alkaline medium, in fact, favors the formation of soluble and/or unstable higher valence hydroxy anions[11,12] that can be assumed to be the causes of film thinning.[11,12] Therefore, on polarizing the electrode at $E = +1.20$ V *vs.* SCE, the following reactions occur in NaOH (1 M):

$$RuO_2 + 4\ OH^- \rightarrow RuO_4^{2-} + 2\ H_2O + 2\ e^- \quad (1)$$

$$RuO_4^{2-} \rightarrow RuO_4^- + e^- \quad (2)$$

$$RuO_4^- + 2\ OH^- \rightarrow RuO_4(OH)_2^- + 2\ e^- \quad (3)$$

$$RuO_4(OH)_2^- \rightarrow RuO_4^- + 2\ H^+ + 2\ e^- + O_{2(g)} \uparrow \quad (4)$$

The production of ruthenate in reaction (1) was, in fact, demonstrated by the orange color that appeared near the electrode during anodic polarization[4] in alkaline media. Synergistically with the partial film dissolution, the oxygen evolution reaction increased the film roughness, as measured by AFM (compared with as-grown sample **1** in Table 1).

In acidic media, the reaction pathway for oxygen evolution does not promote the formation of ruthenate and perrhuthenate.[2,10] Therefore, on polarizing the electrode at $E = +1.20$ V *vs.* SCE in H_2SO_4 (1 M) the following reactions take place:

$$RuO_2 + H_2O \rightarrow RuO_3 + 2\ H^+ + 2\ e^- \quad (5)$$

$$RuO_3 \rightarrow RuO_2 + O_{2(g)} \uparrow \quad (6)$$

In agreement with eqns. (5) and (6), in fact, no orange color, typical of ruthenate formation, was observed during electrochemical processing in acidic media. Therefore, in accordance with literature reports,[10–12] the behavior of the film in H_2SO_4 (1 M) was attributed to the formation of hydrous RuO_2, which dissolved when polarized at +1.2 V.

The RuO_2 electrodes exhibited an appreciable capacitive potential region. On this basis capacitive measurements were performed by means of cyclic voltammetry in the range from +0.35 to −0.05 V, in order to prevent film dissolution, at various scan rates (Fig. 2). After calculating the capacitive current as an average value in the range between +0.14 and +0.27 V, in which no faradic processes occurred, the mean capacity C was estimated using the relationship[13]

$$C = i_c/Av$$

where i_c is the capacitive current, A is the geometrical area of the electrode and v the sweep rate.

The average capacitance calculated in this way was 9.6×10^{-3} F (6.23 mF cm^{-2} by assuming the geometrical area).

For metallic Ru, the preliminary sweeping conditions were very mild (potential range between –0.60 and +0.20 V), in order to prevent undesired oxidation reactions and consequent film dissolution,[12,13] but to obtain the electrochemically active species arising from the oxidation of the Ru surface.[2,11,12] For these films, in fact, the oxidation process in NaOH (1 M) resulted in immediate film dissolution [reaction (1)], indicated by the strong orange color of the solution near the electrode. Therefore, cyclic voltammograms were recorded in NaOH (0.1 M), up to +0.15 V at 5 mV s^{-1}, in order to limit film dissolution (Fig. 3). Before the sweeps, the initial conditions were partially restored by polarizing the film at a cathodic potential of $E = -0.80$ V.

The voltammetric curves were similar to those already observed for nanocrystalline Ru obtained *via* ballmilling.[13] However, capacitive measurements were not possible because the potential region over which capacitive behavior occurred was limited.

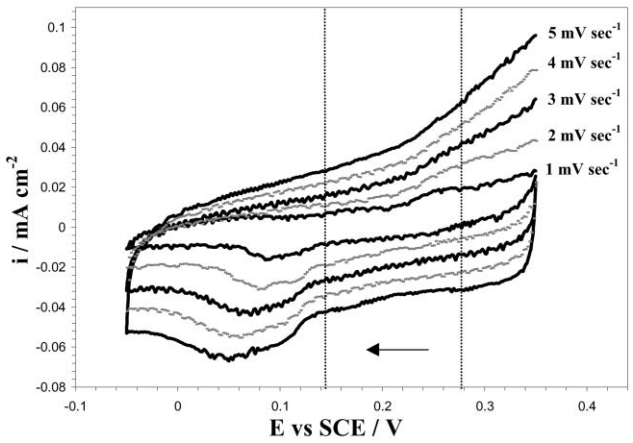

Fig. 2 Cyclic voltammograms in the range from +0.35 to −0.05 V *vs.* SCE at various scan rates (indicated in the figure).

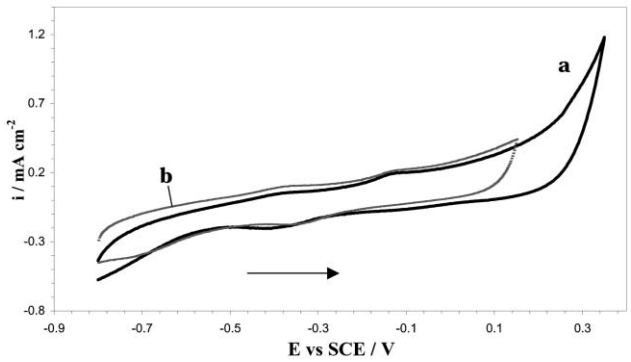

Fig. 3 Cyclic voltammograms of the Ru sample in NaOH (0.1 M) between (a) −0.8 and +0.35 V and (b) −0.8 and +0.15 V ($v = 5$ mV s^{-1}).

X-Ray photoelectron spectroscopy (XPS) analysis

XPS surface analyses of the Ru and RuO_2 samples were complicated by the overlap of the $Ru3d_{3/2}$ signal with the adventitious C1s photopeak,[14] which affected the intensity ratio of the Ru3d spin–orbit components. In particular, the $I_{Ru3d_{5/2}}/I_{Ru3d_{3/2}}$ ratio of lower than 1.5 indicated the presence of carbon.[15] Nevertheless, the rather low distortion of the Ru3d signal for the oxide films was related to the presence of a small amount of carbon contamination.

In Fig. 4a is shown the Ru3d peak for as-grown RuO_2. The presence of ruthenium dioxide was confirmed by the following features.

1) The $Ru3d_{5/2}$ peak had a single component at a BE value of 280.7 eV, according to the literature data.[14]

2) In addition to the 3d components, two broad satellite peaks were present, shifted by +1.8 eV from the principal components. These satellites, attributed to the final state core-hole screening effects, are considered to be a fingerprint for RuO_2;[15]

3) The BE separation between the RuO_2 contribution to the O1s peak (see below) and the $Ru3d_{5/2}$ peak was 248.9 eV, according to earlier data.[16]

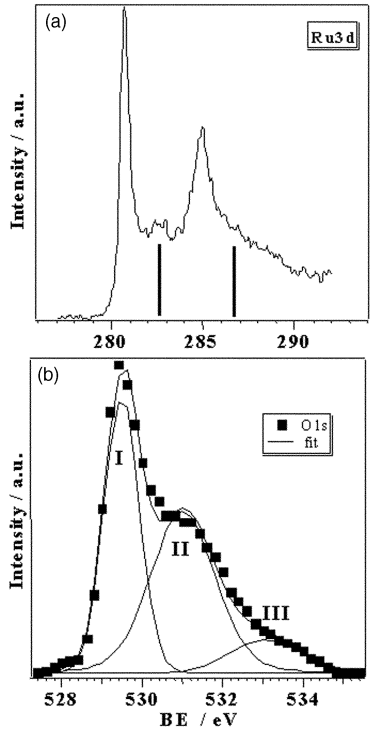

Fig. 4 XPS peaks for an as-grown RuO_2 film. (a) Ru3d peak (the vertical lines indicate the satellite peaks); (b) O1s peak: (I) RuO_2 contribution, (II) hydroxy species and (III) adsorbed water.

Table 2 Surface hydration percentage and O/Ru ratio measured by XPS surface analysis[a]

	O/Ru		
Sample	Before electrochemical test	After electrochemical test	O1s hydration (%)
1	1.9	—	47.7
2	1.9	1.9	45.8
3	1.9	2.2	47.8
4	1.9	2.2	53.7
5	1.9	1.9	50.2
1m	0.8	—	—
2m	0.6	2.5	—
3m	0.4	2.2	—

[a]The degree of hydration of samples **2**–**5** was calculated following the electrochemical processing reported in Table 1.

It can be seen from Table 2 that the O/Ru surface ratio for the RuO_2 films before electrochemical processing was very close to the stoichiometric value. Deconvolution of the O1s peak (Fig. 4b) was performed using three components: the first, at BE ≈ 529.5 eV, was due to the oxide,[17] the second, around 531.1 eV, indicated the presence of hydroxylic groups[18,19] and the third, at BE > 533 eV, was assigned to adsorbed water.[14]

After the electrochemical tests, the chemical state of the Ru oxide films underwent no appreciable changes and the only difference with respect to the as-grown material was the hydrous species content. It can be seen from Table 2 that the surface hydration percentage, calculated by the sum of the –OH and H_2O contributions, was influenced by the electrochemical processing conditions. In particular, the degree of hydration increased for oxide samples polarized at +1.20 V (samples **4** and **5**), irrespective of the electrolytic media.

In the case of the Ru metal films, XPS analyses showed appreciable compositional modifications after the electrochemical tests. The presence of metallic Ru in the as-grown samples was demonstrated by the BE value of the $Ru3d_{5/2}$ peak (≈ 279.9 eV[17,20]) and by the absence of the RuO_2 satellite peaks. The oxygen detected on the surface (see Fig. 5a) could be easily removed after a mild sputtering (5 min, 2 kV), indicating that it arose from interaction with the atmosphere. The $I(Ru3d_{5/2})/I(Ru3d_{3/2})$ ratio was lower than the theoretical value (1.5), due to carbon contamination.[15]

After electrochemical processing (Fig. 5b and Table 2), the Ru films showed a significant increase in oxygen content. In agreement with previous reports,[17,20] this effect was assigned to partial surface oxidation and hydroxylation of metallic Ru. Deconvolution of the Ru3d peak indicated the presence of 65% Ru(0) (279.9 eV) and 35% Ru(IV) (280.7 eV) respectively for all

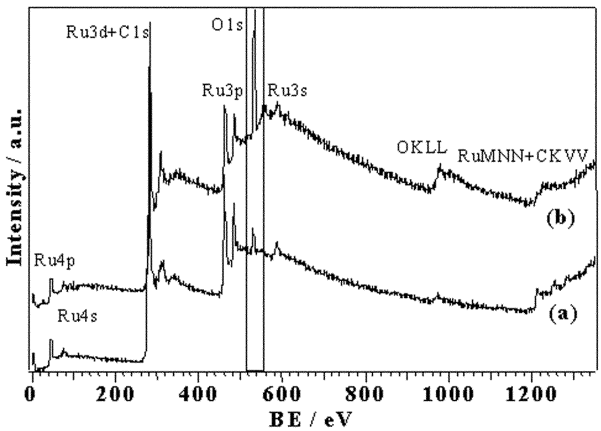

Fig. 5 Survey spectra of the Ru sample: (a) as-grown; (b) after electrochemical processing (sample **2m**).

the examined samples. It is worth highlighting that RuO_2 was produced for all the cycled samples (Table 2), in accord with literature sources on the electrocatalytically active species of the metal surface.[2,13]

Secondary ion mass spectrometry (SIMS) analysis

The high sensitivity of SIMS suggested that this technique would be suitable for detecting local modifications of the composition of the material that can occur on polarization.[7,21]

Analysis of the positive- and negative-ion mass spectra of the as-grown RuO_2 nanocrystalline films showed the presence of Ru^+ and $RuO_x^{+/-}$ isotopic patterns. Ions like $RuC^{+/-}$, $RuCO_x^{+/-}$ and $Ru_2C^{+/-}$ were detected only at trace level, indicating good precursor conversion into the oxide during CVD processing.[6] In Fig. 6 the positive-ion mass spectrum of the film (Fig. 6a) is compared with that recorded at the interface RuO_2–Ti (Fig. 6b). In the spectra recorded in the interface region, higher intensity Ti^+, TiO_x^+, Ti_2^+ and $Ti_2O_x^+$ signals were detected, but they were also present in the surface region spectrum. This effect is related to high surface roughness and/or intermixing phenomena, as previously observed for other substrates.[6] In the low mass portion of the positive-ion spectra, several signals were attributed to inorganic/organic impurities, characterized by high ionic yields, which inevitably contaminate the samples during processing.

In order to distinguish the SIMS behavior of the electrochemically processed RuO_2 films, some convenient signals (selected since they were related with the most abundant isotopes) were followed as a function of the bombarding time.

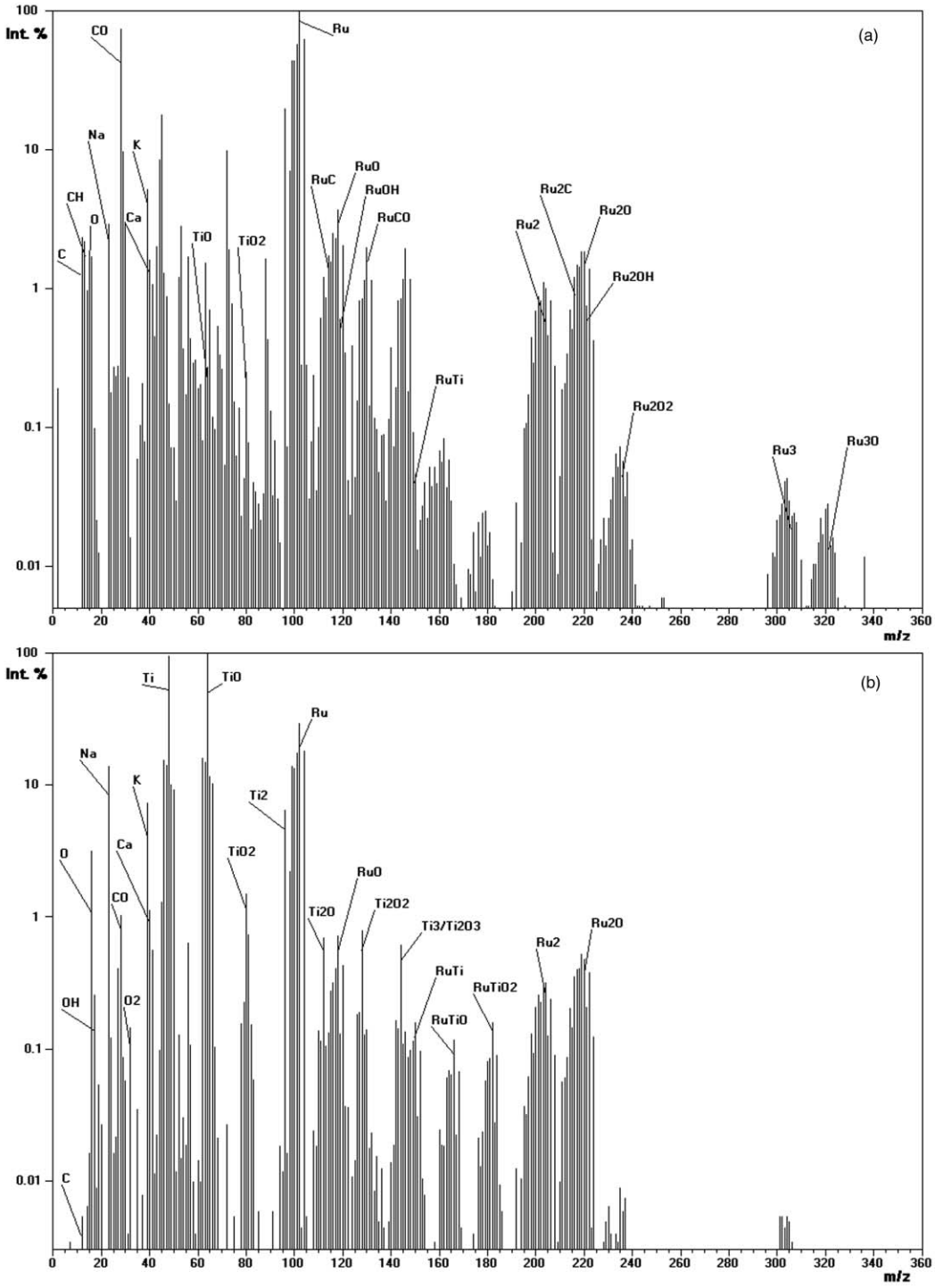

Fig. 6 Positive-ion mass spectra of as-grown RuO_2: (a) surface regions; (b) in the RuO_2–Ti interface region.

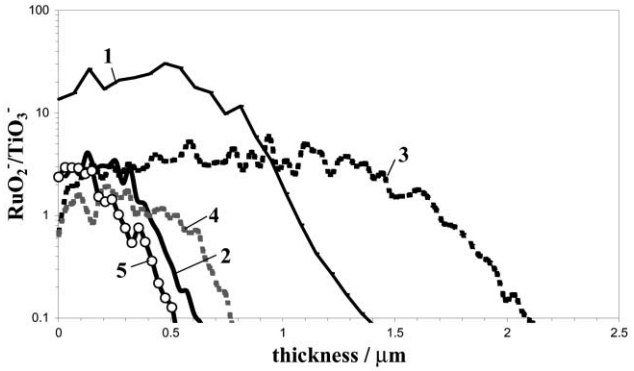

Fig. 7 RuO_2^-/TiO_3^- SIMS in-depth ion intensity ratios for the electrochemically processed RuO_2 samples (see Table 1).

In particular, the SIMS technique enabled us to observe the changes in thickness. In Fig. 7 the RuO_2^- signals, normalized to that of TiO_3^-, are compared for the electrochemically processed samples in either NaOH or H_2SO_4 (1 M).

In observing the sharp decrease in the RuO_2^-/TiO_3^- ratios at the RuO_2–Ti interface, it is noteworthy that sample **3**, cycled in acidic electrolyte, showed a significant increase in film thickness with respect to the other samples, in agreement with the profiler measurements (Table 1) and attributable to the hydration effect, as shown by XPS analyses. Conversely, all the samples processed in NaOH exhibited a film thinning.

Fig. 8 depicts the surface positive-ion mass spectra of both as-grown (Fig. 8a) and cycled (Fig. 8b) Ru metal films. It was interesting to observe that the signals related to the alkaline

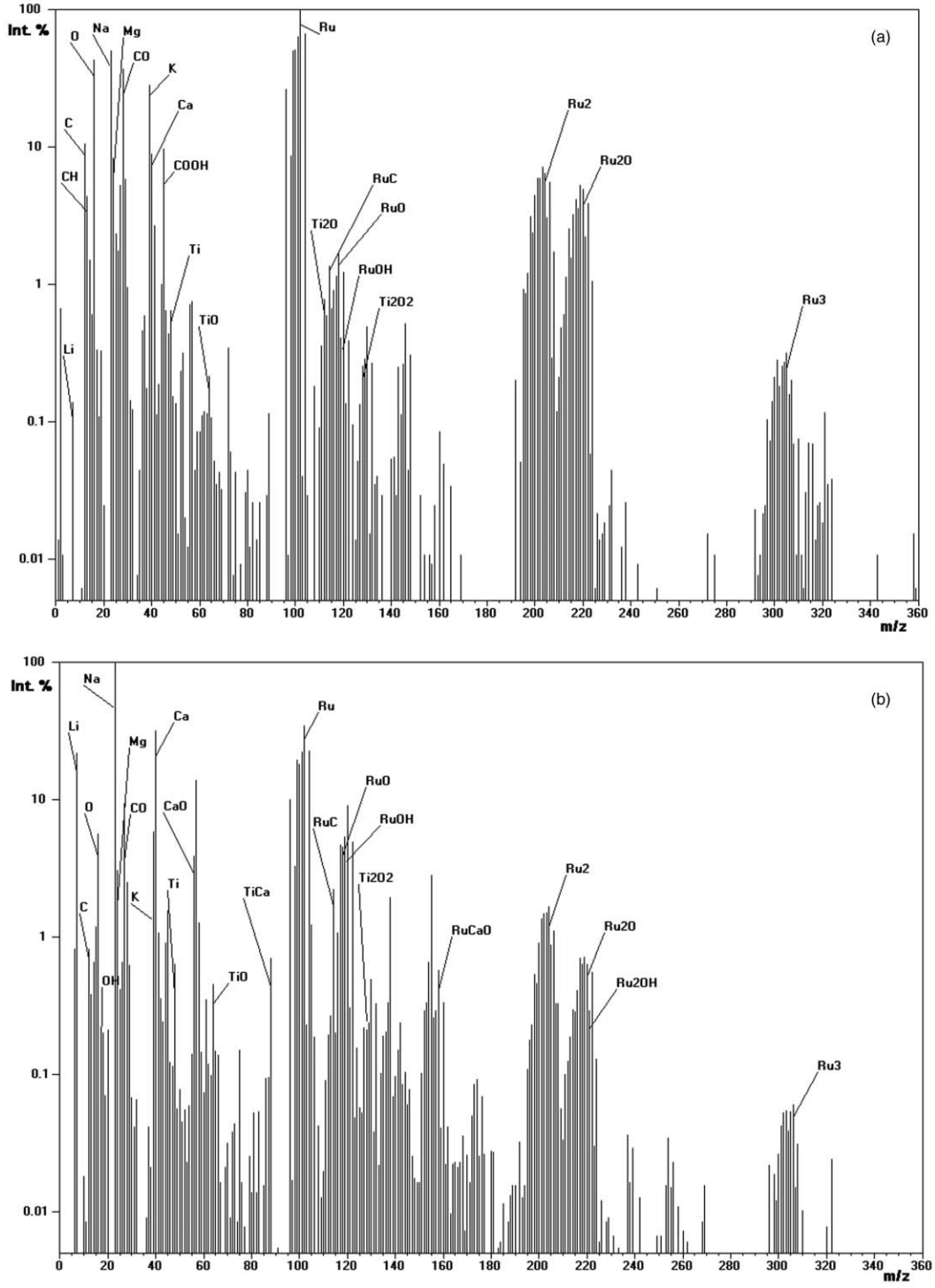

Fig. 8 Surface positive-ion mass spectra of Ru films: (a) as-grown and (b) after voltammetric sweeps.

species, diffused into the film from the electrochemical bath, increased after potential sweeps. Moreover, for the electrochemically-processed sample, the intensity of the RuO^+ species increased at the expense of that of the Ru^+ signal, in agreement with the metal oxidation previously observed by XPS analysis. In addition, many signals for hydrated species ($RuOH^+$, RuO_2H^+, *etc.*) were detected, confirming the surface hydration induced by electrochemical processing.

For the as-grown Ru films (Fig. 9a) constant behavior of the Ru-related signals was observed along the whole film thickness. Conversely, for the cycled Ru (Fig. 9b) the RuO^+ signal showed an appreciable increase in the near-surface region, as expected for the surface oxidation reaction. The lower time necessary to reach the substrate confirmed the partial dissolution of the metal (see Table 1).

Atomic force microscopy (AFM) analysis

After etching in oxalic acid, Ti substrates revealed an increased roughness that had a marked influence on the film morphology, as observed for other substrates.[6] Fig. 10a shows the AFM image of the RuO_2 surface before electrochemical testing (sample **1**). After electrochemical processing (see Fig. 10b and 10c for the RuO_2 films after O_2 evolution in acidic, sample **4**, and in alkaline media, sample **5**, respectively), both the surface roughness and the grain size underwent appreciable increases. The latter effect was more pronounced in acidic media where the hydration phenomena were more relevant, while in alkaline media grain size increase was less marked.

In the case of Ru films (Fig. 11a) no grain structure was detected. After electrochemical processing, appreciable morphology changes were observed (Fig. 11b and Table 1). The presence of small grains was detected, showing a morphology comparable to that of RuO_2. This feature was explained by the surface formation of RuO_2, as observed by XPS analyses.

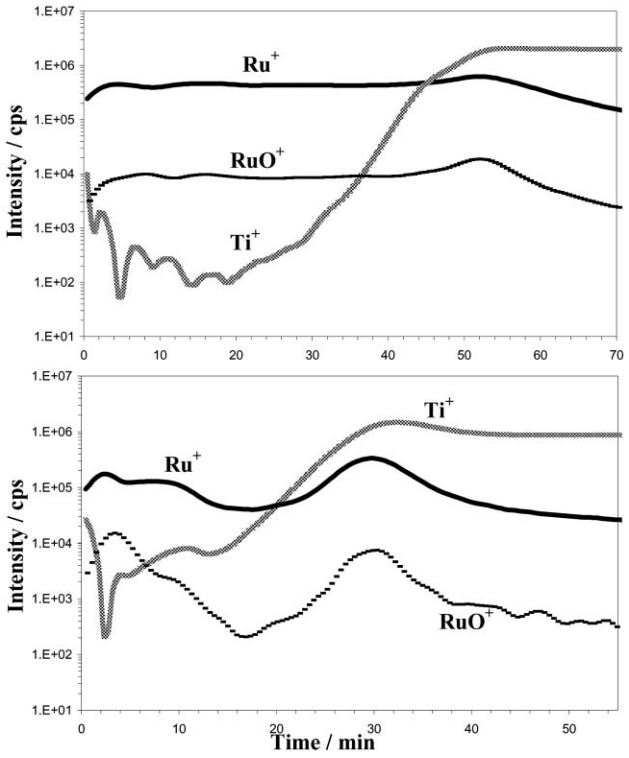

Fig. 9 Ru^+, RuO^+ and Ti^+ distributions as a function of bombarding time for metallic Ru: (a) as-grown and (b) after voltammetric sweeps.

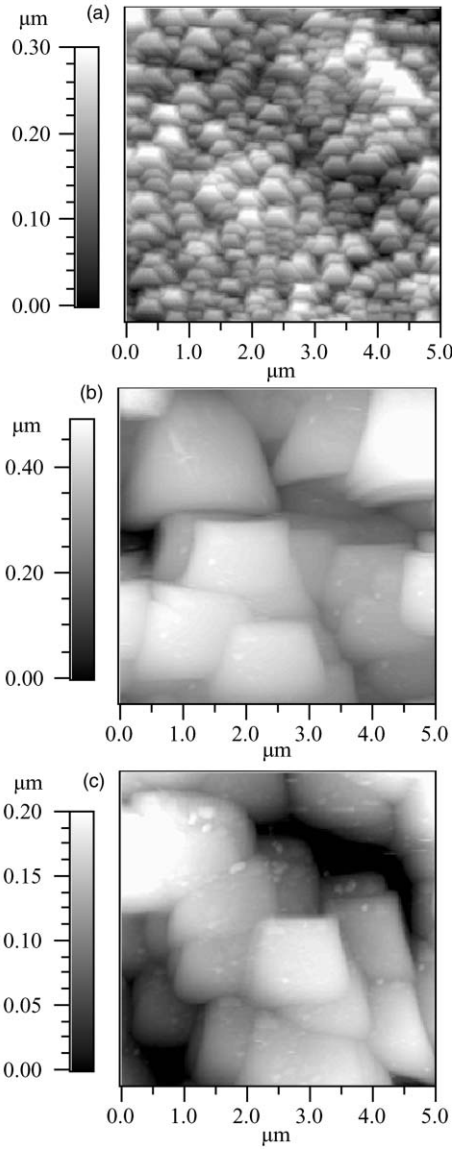

Fig. 10 AFM images of RuO_2 films (a) as-grown (sample **1**); (b) after polarization at +1.2 V in acidic media (sample **4**); (c) after polarization at +1.2 V in alkaline media (sample **5**).

Conclusions

Chemical vapor deposition was proposed as an alternative route for the preparation of Ru and RuO_2 nanophasic thin layers to be used as electrodes in aqueous media. The films were deposited on Ti using the complex $Ru(COD)(\eta^3\text{-allyl})_2$ as precursor and their electrochemical behavior in the initial stage of O_2 evolution was examined under various conditions. Sample characterization *ex situ* was carried out by XRD, XPS, SIMS and AFM, in order to assess the compositional and morphological modifications induced by electrochemical processing.

The obtained results indicate that the CVD RuO_2–Ti nanocrystalline films had electrocatalytic activity towards O_2 evolution and were more stable in acidic than in alkaline media.

Different behavior was observed for Ru electrodes that were cycled under mild conditions in order to limit film degradation. In this case, surface and in-depth analyses confirmed the reproducible formation of oxidized species, in agreement with previous work on polycrystalline electrodes.

As a perspective for future developments, the synthesis of composite oxide system (RuO_2–valve metal oxide) will be attempted in order to improve the performances of these nanocrystalline materials.

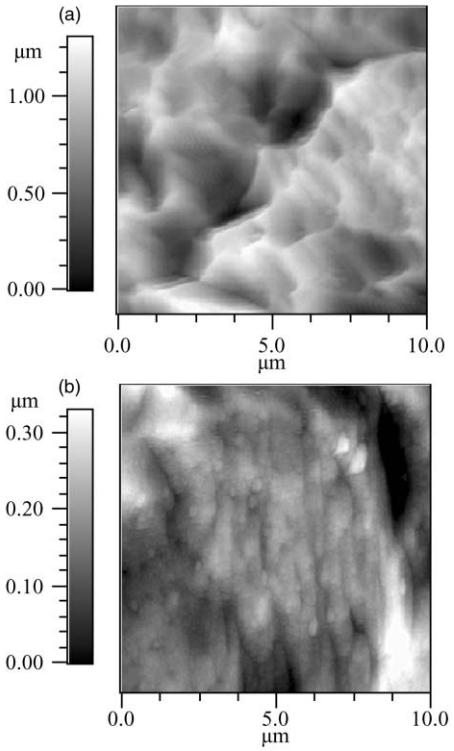

Fig. 11 AFM images of metallic Ru: (a) as-grown (sample **1m**); (b) after voltammetric cycling (sample **2m**).

Acknowledgement

The authors are grateful to Professor Paolo Colombo of Dipartimento di Ingegneria Meccanica, Sezione Materiali, Università di Padova, for the XRD measurements. Progetto Finalizzato ''Materiali Speciali per Tecnologie Avanzate II'' and Programma ''Materiali Innovativi'' (legge 95/95, 5%), funded by CNR, supported the work financially.

References

1 S. Trasatti and G. Lodi, in *Electrodes of Conductive Metallic Oxides, Part A*, ed. S. Trasatti, Elsevier, New York, 1980, p. 301.
2 S. Trasatti, *Chim. Ind. (Milan)*, 1998, **80**, 199.
3 N. Wagner, M. Horx, M. Jacobs and M. Suchi, *Phys. Status Solidi A*, 1987, **101**, K23.
4 L. D. Burke and J. F. Healy, *J. Electroanal. Chem.*, 1981, **124**, 327.
5 K. Kameyama, S. Shohji, S. Onoue, K. Nishimura, K. Yahizokawa and Y. Takasu, *J. Electrochem. Soc.*, 1993, **140**, 1034.
6 D. Barreca, A. Buchberger, S. Daolio, L. E. Depero, M. Fabrizio, F. Morandini, G. A. Rizzi, L. Sangaletti and E. Tondello, *Langmuir*, 1999, **15**, 4537.
7 S. Daolio, J. Kristóf, C. Piccirillo, C. Pagura and A. De Battisti, *J. Mater. Chem.*, 1996, **6**, 567.
8 A. Tolstogouzov, S. Daolio and C. Pagura, *Surf. Sci.*, 1999, **441**, 213.
9 J. Vetrone, C. M. Foster, G. R. Bai, A. Wang, J. Patel and X. Wu, *J. Mater. Res.*, 1998, **13**, 2281.
10 T. R. Jow and L. P. Zheng, *J. Electrochem. Soc.*, 1998, **145**, 49.
11 L. D. Burke, O. J. Murphy, J. F. O'Neill and S. Venkatesan, *J. Chem. Soc., Faraday Trans.*, 1977, **73**, 1695.
12 S. Trasatti and G. Lodi, in *Electrodes of Conductive Metallic Oxides, Part B*, ed. S. Trasatti, Elsevier, New York, 1980, p. 553.
13 L. Roué, M. Blouin and D. Guay, *J. Electrochem. Soc.*, 1998, **145**, 1624.
14 J. F. Moulder, W. F. Stickle, P. W. Sobol and K. D. Bonben, *Handbook of X-ray Photoelectron Spectroscopy*, Perkin-Elmer, Physical Electronics Division, 1992.
15 Y. J. Kim, Y. Gao and S. Chambers, *Appl. Surf. Sci.*, 1997, **120**, 250.
16 D. D. Sarma and C. N. R. Rao, *J. Electron Spectrosc. Relat. Phenom.*, 1980, **20**, 25.
17 R. Kötz, H. J. Lewerenz and S. Stucki, *J. Electrochem. Soc.*, 1983, **130**, 825.
18 T. S. Wittrig, D. E. Ibbotson and W. H. Weinberg, *Surf. Sci.*, 1981, **102**, 506.
19 K. S. Kim and N. Winograd, *J. Catal.*, 1974, **35**, 66.
20 H. J. Lewerenz, S. Stucki and R. Kötz, *Surf. Sci.*, 1983, **126**, 463.
21 S. Daolio, B. Facchin, C. Pagura, A. De Battisti and A. Barbieri, *Rapid Commun. Mass Spectrom.*, 1993, **7**, 887.